LWT - Food Science and Technology 172 (2022) 114241

Contents lists available at ScienceDirect

LWT

journal homepage: www.elsevier.com/locate/lwt

Identification of exudate metabolites associated with quality in beef during refrigeration

Jun Liu [a,1], Ziying Hu [b,1], Anran Zheng [a], Qin Ma [b], Dunhua Liu [a,b,*]

[a] School of Agriculture, Ningxia University, 750021, Yinchuan, China
[b] School of Food & Wine, Ningxia University, 750021, Yinchuan, China

ARTICLE INFO

Keywords:
Metabolomic
Exudates
Beef
Meat quality

ABSTRACT

This study aimed to assess the changes in metabolites from beef exudates (EXU), to reveal the potential of its application in determining beef quality. EXU were collected from 2, 4 and 6 days of chilled meat as a study model. Analysis of the EXU using the UPLC-Q-Exactive-MS platform identified 877 metabolites and 433 differential metabolites (DMs). The DMs mainly included organic acids (45), organoheterocyclic (45), lignans (38), phenylpropanoids and polyketides (22), benzenoids (19), organic oxygen (17), and nucleosides (16). Of these, 75 DMs with a KEGG ID were significantly associated with water retention, colour and shear force in beef ($P < 0.05$). These DMs affected beef quality by participating in metabolic pathways, such as energy, carbohydrate and amino acid metabolism, ferroptosis, apoptosis and oxidative status. Based on the results of the current study, it may be feasible to estimate the quality of meat by analysing its EXU.

1. Introduction

Beef provides many nutrients essential for human health and is considered a high-value meat (An, Nickols-Richardson, Alston, Shen, & Clarke, 2019). However, the consumption choice of beef is usually fresh rather than frozen, which requires beef to maintain excellent quality characteristics during display for sale, in terms of bright red color, little exudates (EXU) production and good flavor (You, Her, Shafel, Kang, & Jun 2020). Meat quality is impacted by numerous extrinsic (post-slaughter temperature, O_2 availability, packaging, etc.) and intrinsic factors (breed, animal age, muscle type, pH value, apoptosis, conversion of aerobic to anaerobic respiration, myogenic fiber contraction, myosin denaturation, etc.) (Kim et al., 2015; Yu et al., 2017). These complex metabolic processes, or pathways, essentially involve a range of proteases and metabolites. Muscle EXU, or meat juice, has been reported to provide valuable information about the storage or ageing process of meat (Di Luca, Elia, Mullen, & Hamill, 2013; Wang, Li, Zhao, Bi, & Xie, 2022).

In the course of chilled transportation or marketing, water is naturally released from the tissues of slaughtered beef to the surface of the meat or the package due to a series of decomposition of muscle fibers, cell membrane structures and intracellular cytoskeleton, forming a collection of juices or EXU (Castejón, García-Segura, Escudero, Herrera, & Cambero, 2015; Liu, Hu, Liu, Zheng, & Ma, 2023). For meat, EXU is unavoidable and may reduce the organoleptic quality of the meat, and decrease meat weight and the levels of nutrients (Xing et al., 2020). EXU is derived from free water in the muscle tissue that is not readily mobile (Bowker, Gamble, & Zhuang, 2016), containing water-soluble sarcoplasmic proteins, heme, nucleotides, peptides, amino acids, soluble enzymes and water-soluble vitamins (Kim et al., 2013). As the variety of metabolite species in EXU is abundant and diverse, its potential utilization has been taken note of by using metabolite fractions in it to study meat quality, including freshness, tenderness, color, water-holding capacity, protein and lipid oxidation, and microbial metabolism. (Castejón, Escudero, Herrera, & Cambero, 2015; Kim et al., 2013; Xing et al., 2020).

EXU, as an easily accessible metabolite or analytical material, can effectively provide complex biological information about the sample, providing comprehensive sample information on meat quality and underlying mechanisms (Zhou et al., 2019). A promising histological strategy combined with bioinformatics, namely metabolomics, offers a new perspective to illustrate the underlying mechanisms and discover

* Corresponding author. Room 320, School of Agriculture, Ningxia University Helanshan Campus, Mount Helan West Road, Xixia District, Yinchuan City, 750000, Ningxia, China.
E-mail addresses: ldh320@nxu.edu.cn, dunhualiu@126.com (D. Liu).
[1] These authors contributed equally to this work.

https://doi.org/10.1016/j.lwt.2022.114241
Received 1 August 2022; Received in revised form 20 November 2022; Accepted 29 November 2022
Available online 30 November 2022

potential biomarkers to improve meat quality, being a critical tool to reveal the biochemical changes occurring at the metabolite level in meat aging (Wang et al., 2022; Yu, Cooper, Sobreira, & Kim, 2021). In conclusion, EXU can provide information on meat quality for unraveling potential mechanisms of beef quality changes. To our knowledge, there are no studies on the use of metabolomics to reveal the metabolite profile of beef EXU. Given the intricacy of the beef storage process at the physiological and molecular levels, this study aimed to determine metabolites in EXU and potential mechanisms affecting meat quality changes during beef refrigeration at 4 °C for 2, 4, and 6 days using ultra-performance liquid chromatography coupled with Q Exactive hybrid quadrupole-Orbitrap mass spectrometry (UPLC-Q-Exactive MS) non-targeted metabolomics to provide a theoretical basis for refrigerated transportation of livestock products.

2. Materials and methods

2.1. Raw materials

Eight male yellow cattle from a farm in China (Qinchuan cattle, 18–24 months old, body weigh 400 ± 20 (SD) kg) were slaughtered at a local slaughterhouse in Ningxia (Yitai Herding Co., Yinchuan, China) according to the guidelines of the Canadian Council on Animal Care (CCAC) & the Assessment Program of the CCAC (2000). Following cattle exsanguination, a sample of approximately 500 g of M. longissimus lumborum muscles (loins) (from the twelfth thoracic vertebrae to the fifth lumbar vertebrae, as this part is homogeneous and easy to collect) was immediately obtained, placed in a polyethylene self-sealing bag in a foam box filled with ice packs, and a plastic divider in the middle, and transported to the laboratory within 3 h. The muscle samples were divided into three groups (n = 6) after being sliced into pieces with a thickness of 2.5 cm, an average weight of 100.0 ± 2.5 g and a consistent shape. The muscles were put onto a PET plastic tray (length, 195 mm; height, 30 mm; width, 145 mm), and wrapped with polyvinyl chloride film. Muscles were displayed for 6 days at 4.0 ± 0.5 °C in an open-front refrigerated display case (XR150D, Foshan City Aslok Refrigeration Equipment Co., Ltd., Foshan, China) with a single shelf and a 30-degree tilt at the bottom, as after 6 days the microbial infection exceeded the standard the beef may not be suitable for consumption (Ayaka et al., 2022; Fang, Feng, Lu, & Zhu, 2022). Muscles were placed randomly and rotated twice daily to obtain random sample placement. All muscle exudates were collected from the bottom of the tray with a medical disposable syringe on days 2, 4 and 6 of the storage, defined as EXU2, EXU4 and EXU6. The exudates were put into 2 mL lyophilisation tubes and quickly frozen using liquid nitrogen, and then rapidly transferred to a medical cryostat storage chamber (DW-86L486, Qingdao Haier Biomedical Co., Qingdao, China) at −80 °C. Muscle samples were taken from the center of the meat, defined as day 2, day 4, and day 6, and fresh samples were used for meat quality analysis.

2.2. Evaluation of beef quality

The beef color change was estimated by a handheld colorimeter (CR-410, Minolta Co., Ltd., Suita, Osaka, Japan), and the results were expressed as L^* (lightness), a^* (redness) and b^* (yellowness), with a total of six measurements for each sample. Calibration was carried out before each test using the white standard plate provided by the manufacturer. The water-holding capacity was expressed by purge loss (PL), centrifugal loss (CL) and weight loss after centrifugation (Liu, Liu, Zheng, & Ma, 2022; Nour, 2022), with slight modifications. Fresh bovine muscle was weighed (initial weight) and placed in a sealed polythene bag. After storage at 4 °C for 24 h, excess water was wiped from the surface and the sample was re-weighed (final weight). PL was expressed as a percentage of weight loss. A 2 ± 0.25 g muscle sample was wrapped in 4 layers of filter paper and centrifuged at 1500×*g*, 4 °C for 5 min. CL was expressed as a percentage of weight loss before and after centrifugation. The muscle samples were placed in a boiling water bath until the internal temperature reached 70 °C. Parallel to the muscle fiber orientation, the meat samples were trimmed to a size of 1.0 cm × 1.0 cm × 3.0 cm, and the beef shear force was measured by using a TA-XT plus texture analyzer (Stable Micro Systems Ltd., Godalming, UK) (Li, Zhang, et al., 2021). The pH value of beef was determined using a calibrated digital portable meat pH meter with a puncture electrode (Testo 205, Testo AG, Lenzkirch, Germany).

2.3. Histomorphological observation

The muscle was trimmed into uniformly sized blocks (0.2 × 0.2 × 0.2 cm^3) and fixed in 4% paraformaldehyde solution for 24 h. The muscle was then embedded in paraffin, sectioned using a pathological slicer (R139, Hubei Taiwei Technology Industry Co., Xiaogan, China), and then stained with hematoxylin and eosin for histological studies. Stained tissue sections were observed using a light microscope (CX33, Olympus Co., New York, USA) (Liu et al., 2022).

2.4. Antioxidant activity analysis of EXU

The activities of total superoxide dismutase (T-SOD, A001-3-2) and glutathione peroxidase (GSH-PX, A005-1-2), and the contents of malondialdehyde (MDA, A003-1-2) and carbonyl (A103-1-1) were determined spectrophotometrically using the assay kits from Nanjing Jiancheng Bioengineering Institute (Nanjing, China).Briefly, the pretreated samples were reacted sequentially with the reagents in the kits according to the detailed instructions included in each kit. The absorbance values were then measured at 450 nm, 412 nm, 532 nm, and 370 nm respectively.

2.5. Untargeted metabolomics analysis based on UHPLC-QTOF-MS

2.5.1. EXU sample pre-treatment

The EXU samples were thawed in an ice bath. Then 100 μL thawed samples were added to 100 μL of −20 °C pre-cooled ultrapure water and 800 μL of −20 °C pre-cooled methanol/acetonitrile (1:1, *v/v*), vortexed and mixed. The samples were sonicated in an ice water bath (40 kHz, 60 min), left to stand for 1 h at −20 °C, and then centrifuged at 16,000×*g*, 4 °C for 20 min. The supernatant (150 μL) was aspirated by syringe and filtered using a 0.22 μm organic phase pinhole filter, aspirated with a micro spray and filtered again, then transferred to a brown bottle feeder vial for storage at −80 °C in the dark. Quality control samples consisted of an equal volume mixture of EXU from all samples.

2.5.2. UHPLC-MS/MS analysis

Untargeted metabolomics analysis was performed by UPLC-Q-Exactive MS with electrospray ionization (ESI) source, in both positive and negative ion modes. Chromatographic separations were accomplished using an Ultimate 3000 UHPLC system (Thermo Scientific, San Jose, CA, USA) on a Hypersil Gold column (100 mm × 2.1 mm, 5 μm, Thermo Scientific). UHPLC conditions: injection volume 3 μL, column temperature 25 °C; mobile phases: water and 25 mM ammonium acetate (A), acetonitrile (B); flow rate: 0.3 mL/min; gradient elution: 0–1 min, 95% B; 1–7 min, 65% B; 7–10.5 min, 35% B; 10.5–15 min, 95% B.

Mass spectrometry was performed on a QE Plus mass spectrometer (Thermo Scientific, San Jose, CA, USA). Mass spectrometry conditions: Electrospray ionization (ESI) source, Data collection in positive ion (+) and negative ion (−) modes. Mass spectrometry parameters: Spray voltage: 3.8 kv (+) in positive ion mode and 3.2 kv (−) in negative ion mode; Capillary temperature: 320 °C (±); Sheath Gas: 30 Arb (±); Aux Gas: 5 Arb (±); Probe heater temperature: 350 °C (±); S-Lens RF Level: 50; Low collision energy 15 eV, High collision energy 60 eV. Mass spectrometry acquisition time: 12 min; parent ion scan range: 80–1200 m/z; primary mass spectrometry resolution: 70,000 @ m/z 200, secondary mass spectrometry resolution: 17,500 @ m/z 200.

Table 1
Changes in meat quality during cold storage.

Parameters	Day		
	2	4	6
L^*	35.07 ± 1.65 [a]	32.95 ± 1.34 [b]	30.94 ± 1.86 [c]
a^*	20.45 ± 1.23 [a]	15.66 ± 1.45 [b]	12.42 ± 1.43 [c]
b^*	5.68 ± 0.84 [a]	4.41 ± 0.81 [b]	3.24 ± 0.65 [c]
Shear force (N)	93.45 ± 4.78 [b]	106.41 ± 3.27 [a]	99.21 ± 1.88 [b]
Centrifuging loss (%)	3.18 ± 0.17 [c]	6.14 ± 0.25 [a]	4.38 ± 0.88 [b]
Purge loss (%)	0.64 ± 0.04 [c]	0.79 ± 0.07 [b]	1.02 ± 0.09 [a]
pH	5.69 ± 0.02 [a]	5.53 ± 0.03 [b]	5.57 ± 0.02 [b]

[1]Results are expressed as mean ± standard error. Means differ for different letters ($P < 0.05$).

2.6. Statistical analysis

Results were expressed as mean ± standard deviation. Data were analysed using one-way analysis of variance (ANOVA) with SPSS 25 (IBM, NY, USA) software. A $p < 0.05$ was significantly different. For non-targeted metabolomics, R (version:4.0.3) and R package were used for all multivariate data analyses and modeling. Data were mean-centered using Pareto scaling. Models were built on principal component analysis (PCA), orthogonal partial least-square discriminant analysis (PLS-DA) and partial least-square discriminant analysis (OPLS-DA). All the models were tested for over fitting with methods of permutation tests.

The discriminating metabolites were obtained using a statistically significant threshold of variable influence on projection (VIP) values obtained from the OPLS-DA model and two-tailed Student's *t*-test (*p* value) on the normalized raw data at univariate analysis level. Metabolites with VIP values greater than 1.0 and *p* values less than 0.05 were considered to be statistically significant metabolites. Fold change was calculated as the logarithm of the average mass response (area) ratio between two arbitrary classes. In addition, the identified differential metabolites were used to perform cluster analyses with R package.

Biological pathways were analysed for differential metabolite data using the KEGG database (http://www.kegg.jp). The enrichment analyses were carried out with the Fisher's exact test, and FDR correction for multiple testing was performed. A $p < 0.05$ was considered statistically significant. Plotting was performed using Origin 2021b software (OriginLab Inc., Northampton, USA).

3. Results and discussion

3.1. Beef quality

Meat quality parameters comprising color, shear force and water-holding capacity (purge loss and centrifuging loss) were assessed. As shown in Table 1, the color instability increased from day 2 to day 6, precisely L^*, a^* and b^* values significantly decreased with muscle color changing from bright red to dark red ($p < 0.05$). This may be due to the loss of pigment resulting from the oxidation of myoglobin and oxymyoglobin to methemoglobin (Coll Cárdenas, Andrés, Giannuzzi, & Zaritzky, 2011). The shear force and CL showed a maximum on day 4, and was significantly higher at day 4 and day 6 than at day 2 ($p < 0.05$). PL tended to increase during storage ($p < 0.05$). The pH values decreased from day 2 to day 4, but increased at day 6. The SF, driven by calpain activity, decreased with storage time to limit the ability of calpain (Dransfield, 1994), an enzyme that can directly hydrolyze myofibrillar proteins depending on a specific calcium concentration and pH value (Gap-Don, Seung, Eun-Young, Sumin & Sun, 2021). Likewise, when the pH value approached the isoelectric point of structural proteins, the proteins also underwent increased denaturation or degradation, then the capillaries between actin and myosin filaments lost their ability to retain water. This may account for the opposite trend of pH levels concerning SF and CL, which coincide with those of Benjamin, Cassius, Stephen, Matthew, and David (2017). In conclusion, the mass

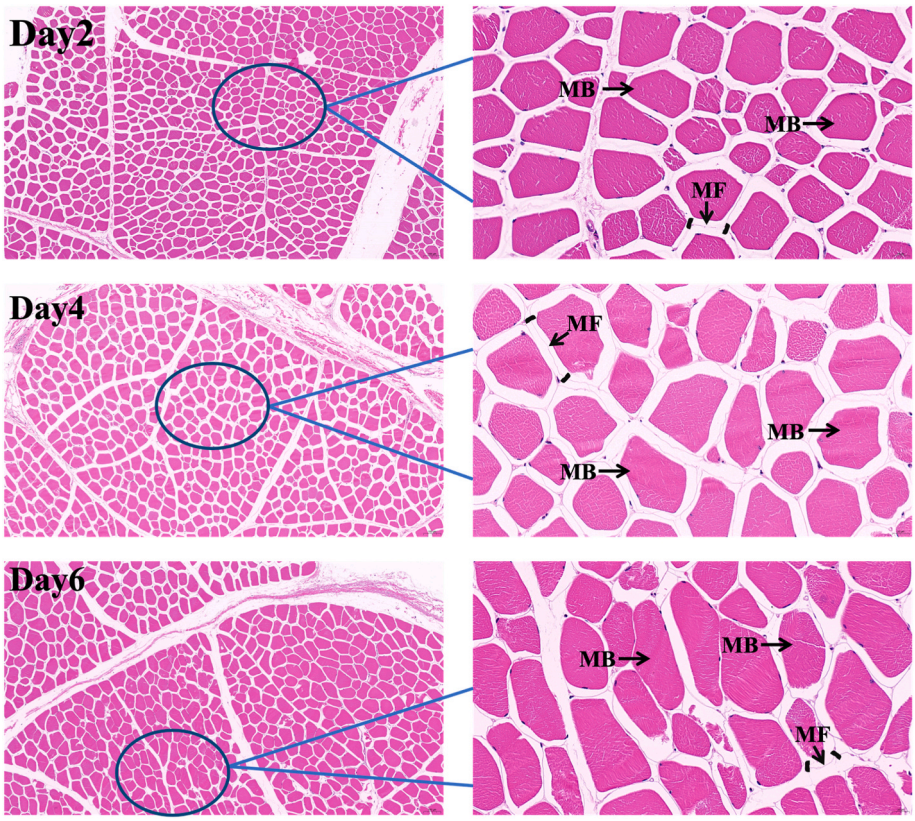

Fig. 1. Histomorphological map of bovine muscle fibers. MB represents muscle fiber bundles, MF represents myofilm. Scale bars: 100 μm and 20 μm.

Table 2
Changes in oxidation index of EXU.

Indicators	EXU2	EXU4	EXU6
SOD (U/mg prot)	4.59 ± 0.46 [a]	3.87 ± 0.19 [b]	3.50 ± 0.13 [c]
GSH-PX (U)	362.01 ± 32.89 [a]	179.06 ± 19.12 [b]	138.89 ± 11.77 [c]
MDA (nmol/mg prot)	0.19 ± 0.02 [c]	0.20 ± 0.01 [b]	0.25 ± 0.00 [a]
Carbonyl (nmol/mg prot)	7.98 ± 0.98 [c]	13.17 ± 1.34 [b]	19.21 ± 2.61 [a]

[1]Results are expressed as mean ± standard error. Means differ for different letters ($P < 0.05$).

changes that occur in beef during refrigeration were closely related to the metabolism in the muscle.

3.2. Histomorphological observation

Morphological changes of the muscle fiber bundles (MB) in the beef were observed by HE staining. As shown in Fig. 1, the MB was neatly arranged and uniformly dense, mainly composed of different types of myofibrillar proteins to maintain the orderly arrangement of muscle cells (Bai, Yin, Ru, Tian, Li, Zhang, Chen, Chai, Xiao, Zhu & Zhao, 2022). On day 2 and day 4, the myofilm (MF) was homogenously wrapped by the MB in the center of the MF with structural integrity. On day 6, however, the muscle membrane was deformed, the muscle spacing continuously diminished and the MB showed structural damage. These results indicated that the strength of the MB gradually decreased as the storage time increased, which may facilitate the effusion of EXU. Another possibility is that oxidative stress in myofibrillar proteins during beef storage may affect water-protein interactions, resulting in reduced water holding capacity of beef (Mariana, David, & Mario, 2014). Collectively these changes were inextricably linked to the complex biochemical reactions within beef.

3.3. Antioxidant activity

SOD and GSH-PX activities were used to assess the oxidative status of EXU. As shown in Table 2, both the activities of SOD and GSH-PX tended to decrease during refrigeration ($p < 0.05$). These endogenous antioxidant enzymes were implicated in the protection against oxidative damage during storage of meat (Pastsart al., 2013). The contents of MDA and carbonyl were used to assess lipid and protein oxidation in EXU respectively. As expected, MDA and carbonyl content increased in the EXU ($p < 0.05$). They were derived from polyunsaturated fatty acids, the N-terminal end of peptide chains or the ε-amino group of lysine residues in proteins, and the oxidative breakdown of various proteins, which were evidence of oxidation within the muscle (Liu, Zhang, Song, Gao, Zheng, Tan, Luo, Li, Hui, & Hong, 2022). Castejón et al. (2015) used NMR spectroscopy to analyze beef exudate and found a large number of free amino acids, and inferred that protein hydrolysis may have begun

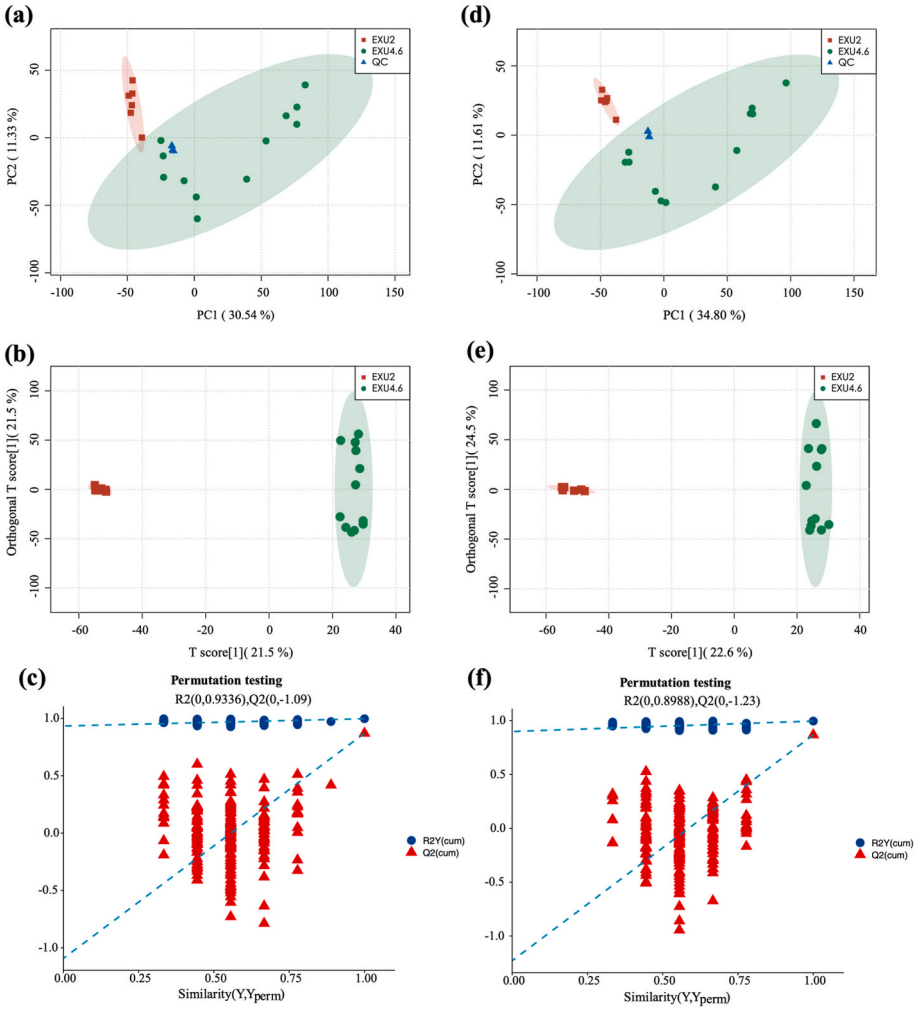

Fig. 2. Multivariate analysis of PCA and OPLS-DA for exudate metabolomics data. (a) PCA score plot for exudate metabolites in positive ion mode; (b) OPLS-DA score plot for exudate metabolites in positive ion mode; (c) OPLS-DA substitution test plot in positive ion mode; (d) PCA score plot for exudate metabolites in negative ion mode; (e) OPLS-DA score plot for exudate metabolites in negative ion mode; (f) OPLS-DA substitution test plot under negative ion mode.

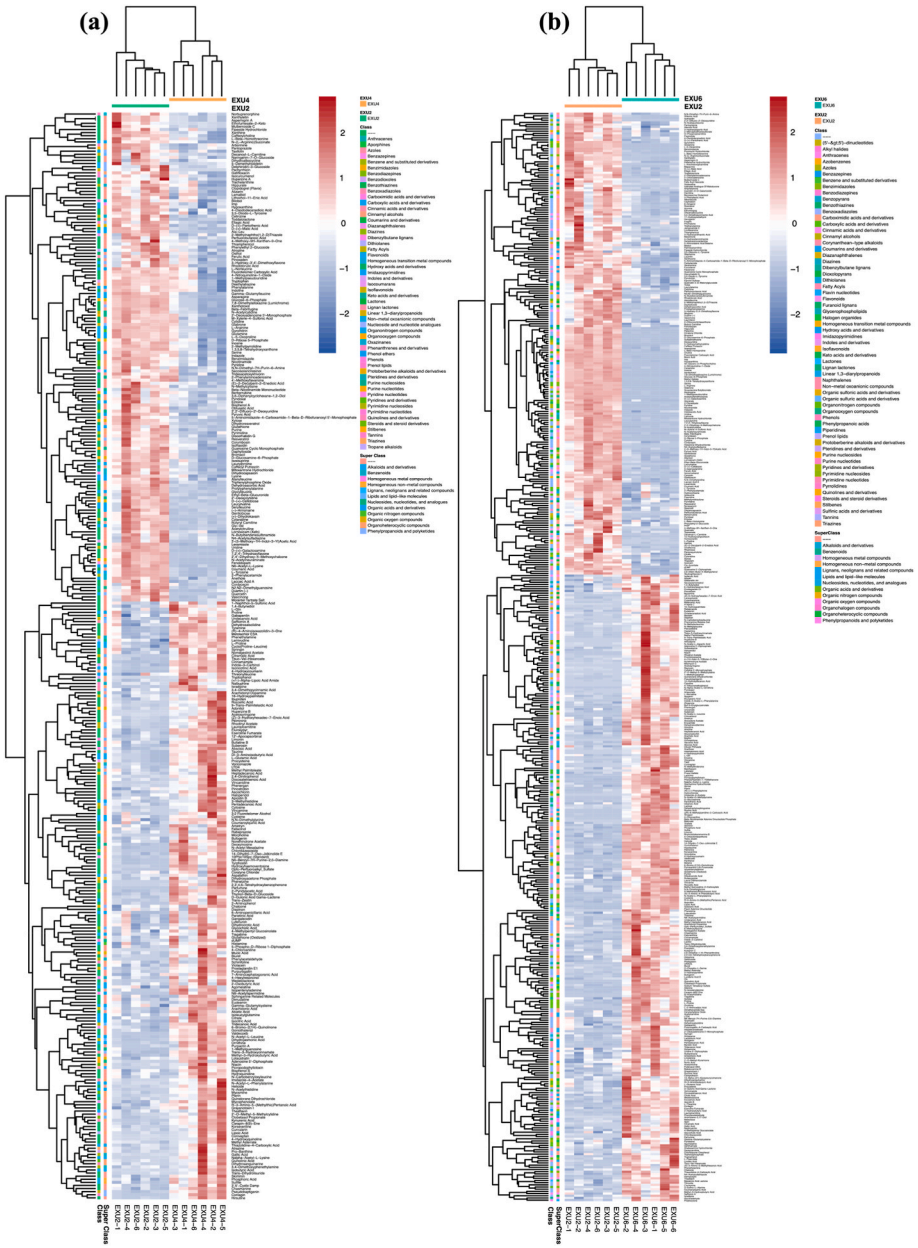

Fig. 3. (a) Cluster heat map analysis of DMs for EXU2 and EXU4 (351 DMs); (b) Cluster heat map analysis of DMs for EXU2 and EXU6 (498 DMs).

since slaughter, in addition to muscle autoxidation, resulting in the accumulation of short-chain fatty acids. In summary, the antioxidant capacity was reduced and the oxidative stress was enhanced in the muscle during refrigeration.

3.4. EXU metabolism

There were 572 and 305 DMs identified in positive and negative mode, respectively. The results of EXU metabolic analysis were visualized by PCA. The quality control samples were distributed in different quadrants in both modes, indicating that there were contrasts somewhere in the range of EXU2/4/6 metabolites, and there was a partial overlap between the samples (Fig. 2a and d). Therefore, a further supervised discriminant statistical analysis method, OPLS-DA was used to eliminate the influence of irrelevant factors in the experimental data. OPLS-DA showed that the sample differences were reduced within the parallel sample groups and between-group differences significantly increased compared with PCA, and EXU2 completely separated from EXU4/6 (Fig. 2b and e). In addition, to avoid overfitting and random effects, the OPLS-DA model was tested with 200 permutations to enhance the predictive power. As shown in Fig. 2 c and f, the horizontal coordinates in the plot represented the sample retention in the replacement test, and the points with a retention rate equal to 1.0 were R2Y and Q2 of the original OPLS-DA model. The parameters R2Y and Q2 in both ion models were >0.5 (positive ion: R2Y = 0.997, Q2 = 0.870; negative ion: R2Y = 0.996, Q2 = 0.868), and the Q2 regression line intercept was lower than 0, indicating that the model was not overfitted. Generally, our results showed good predictability and reliability.

3.5. Selection and identification of differential metabolites

Based on the above results, VIP >1 and $p < 0.05$ were considered as DMs. Fig. 3a and b showed the DMs identified for EXU2, EXU4, and EXU6 in POS and NEG, respectively, with a total of 351 DMs identified in EXU2 and EXU4, and 498 DMs in EXU2 and EXU6. In addition, the clustering heat map revealed variations in DMs clustered in a cluster

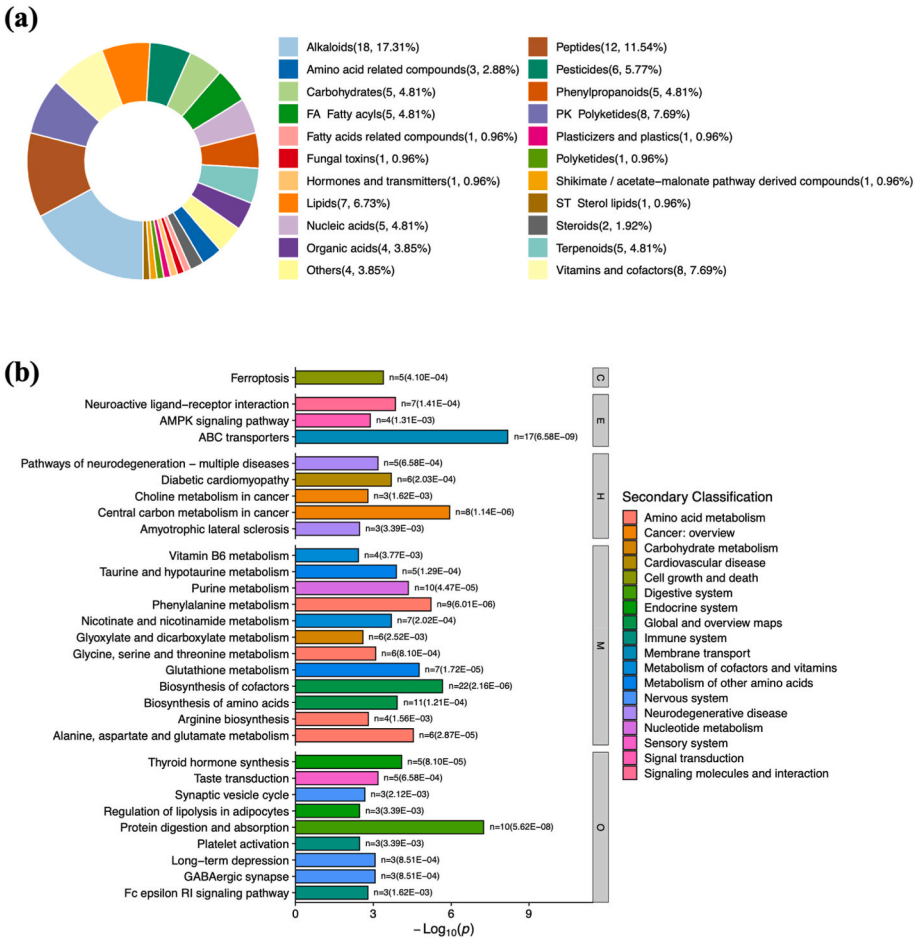

Fig. 4. (a) Loop diagram of differential metabolite classification (KEGG). (b) KEGG pathway enrichment histogram (up to top30, different colors belong to level 2 classification). Information processing (E). Cellular processes (C). Organismal systems (O). Human diseases (H). Drug development (D). (For interpretation of the references to color in this figure legend, the reader is referred to the Web version of this article.)

with similar expression patterns that may be involved in similar cellular metabolic pathways. The clustering analysis showed the classes of DMs identified by KEGG analysis mainly included alkaloids, amino acids, carbohydrates, fatty acids, hormones, conductive substances, lipids, nucleic acids, organic acids and peptides. The results showed that the EXU contained a variety of metabolites, with a significant increase in metabolite differences with storage time, indicating its potential value in revealing changes in beef quality.

3.6. DMs and metabolic pathways

As shown in Fig. 3, the number of DMs and the metabolic pathways involved increased with the increase in the refrigeration time. A total of 433 DMs were identified in EXU4/6 compared to EXU2. The enrichment of these DMs into the KEGG database identified a total of 213 DMs. As shown in Fig. 4a, these DMs mainly consisted of organoheterocyclic compounds, organic acids and their derivatives, lipids and lipid-like molecules, phenylpropanoids and polyketides, benzenoids and nucleosides, nucleotides and their analogues. The main pathways involved (top 30) included cellular processes (C, iron death), environmental information processing (E, ABC transporters and neuroactive ligand-receptor interactions), disease (H, carbon metabolism), metabolism (M, amino acid biosynthesis, cofactor biosynthesis, phenylalanine metabolism and purine metabolism) and organismal systems (O, protein digestion and absorption) (Fig. 4b). A total of 42 metabolic pathways were significantly enriched, including 75 DMs related to beef quality or metabolites.

The metabolism of the muscle cells, and physicochemical and structural alterations in the muscle progenitor fiber are the main contributors to meat quality deterioration (Yu et al., 2021). As shown in Table 3 and Table 4, these DMs affected beef quality by participating in 42 metabolic pathways. Then the correlations among EXU, meat quality and DMs were analysed to assess potential metabolites and metabolic pathways affecting beef quality. Beef oxidation increased beef color instability and moisture loss ($p < 0.05$) (Fig. 5). Beef shear force exhibited a significant correlation with pH value ($p < 0.05$), with no correlations with color and water-holding capacity ($p > 0.05$). Amino acids, oligopeptides, nucleotides and their derivatives in fresh meat may affect the flavor, color, tenderness and water-holding capacity. Notably, alterations in muscle metabolites are the primary driver of changes in tenderness, including creatinine, creatine, myostatin and conjugated linoleic acid in muscle, while the disintegration of myofibrillar proteins can also improve the water-holding capacity of proteins (Pereira, Fernandes, Oliveira, Cnsolo, & Gandra, 2020). Our results suggested that the differential metabolites were significantly correlated with the color, water-holding capacity and meat tenderness.

3.6.1. Energy and carbohydrates

Energy metabolism is the most fundamental feature that sustains cellular life activities. As shown in Table 4, there were a total of five energy metabolism and carbohydrate metabolic pathways with enrichment, including oxidative phosphorylation, sulfur metabolism, citric acid cycle, glyoxylate metabolism, dicarboxylic acid metabolism and butyrate metabolism. Compared to the living body, the aerobic metabolism of the cells gradually changes to anaerobic metabolism during

Table 3
KEGG enriches for differential metabolites (DMs) involved in metabolic pathways.

No.	Formula	Metabo Name	Alignment ID	KEGGID	EXU2 Log10	EXU4 Log10	EXU6 Log10	*P* value	VIP	Log2 FC	KEGG SuperClass
1	C6H10N2O2	Xanthotoxol	P2857	C06231	8.894 ± 0.092	8.701 ± 0.082	8.675 ± 0.071	0.000	1.614	0.693	Amino acids, peptides, and analogues
2	C8H11N	Tridecanoic Acid	N2377	C05332	6.905 ± 0.356	7.614 ± 0.078	7.877 ± 0.247	0.002	1.488	−2.559	Amino acids, peptides, and analogues
3	C11H13NO3	Methyl Gallate	P2496	C03519	6.072 ± 1.009	7.348 ± 0.342	8.534 ± 0.139	0.028	1.092	−5.778	Amino acids, peptides, and analogues
4	C10H18N4O6	1-Methylpseudouridine	N3216	C03406	8.118 ± 0.108	7.484 ± 0.491	7.094 ± 0.075	0.000	1.732	2.070	Amino acids, peptides, and analogues
5	C5H7NO3	Atrazine	P2666	C01879	10.095 ± 0.050	8.879 ± 0.993	7.133 ± 0.156	0.000	1.929	2.877	Amino acids, peptides, and analogues
6	C9H9I2NO3	Eicosenoic Acid	N4009	C01060	8.381 ± 0.019	8.332 ± 0.039	8.211 ± 0.056	0.003	1.434	0.343	Amino acids, peptides, and analogues
7	C4H9NO2	Nalpha-Acetyl-L-Lysine	P2156	C01026	8.769 ± 0.068	8.876 ± 0.017	9.025 ± 0.064	0.003	1.436	−0.617	Amino acids, peptides, and analogues
8	C5H11NO2	Caffeoylcholine	P3640	C00719	10.762 ± 0.008	10.785 ± 0.044	10.894 ± 0.024	0.015	1.209	−0.273	Amino acids, peptides, and analogues
9	C8H14N2O5S	Docosatetraenoic Acid	N4288	C00669	6.464 ± 0.283	6.734 ± 0.107	6.898 ± 0.163	0.023	1.156	−1.044	Amino acids, peptides, and analogues
10	C8H11NO	1,3,5,8-Tetrahydroxyxanthone	P3909	C00483	8.975 ± 0.193	10.031 ± 0.069	9.265 ± 1.379	0.002	1.461	−2.564	Amino acids, peptides, and analogues
11	C5H9N3	N2, N2-Dimethylguanosine	N4018	C00388	8.976 ± 0.046	9.039 ± 0.030	9.109 ± 0.051	0.004	1.324	−0.328	Amino acids, peptides, and analogues
12	C3H6O4	Trigonelline	P967	C00258	9.773 ± 0.075	9.655 ± 0.154	8.344 ± 0.474	0.010	1.238	1.174	Amino acids, peptides, and analogues
13	C5H9NO2	Dimethenamide Esa	N4133	C00148	9.732 ± 0.057	9.882 ± 0.028	10.095 ± 0.088	0.003	1.384	−0.899	Amino acids, peptides, and analogues
14	C9H11NO3	4′-Methoxyflavanone	N3137	C00082	9.663 ± 0.066	9.017 ± 0.128	9.109 ± 0.305	0.000	1.934	1.786	Amino acids, peptides, and analogues
15	C5H10N2O3	Polygalic Acid	P6145	C00064	6.944 ± 0.237	7.340 ± 0.177	7.369 ± 0.234	0.010	1.245	−1.287	Amino acids, peptides, and analogues
16	C6H14N4O2	Huperzine B	P3862	C00062	10.203 ± 0.024	9.322 ± 0.571	8.637 ± 0.112	0.000	1.966	2.742	Amino acids, peptides, and analogues
17	C5H9NO4	Cephalexin	P4853	C00025	9.799 ± 0.178	10.404 ± 0.122	10.094 ± 0.096	0.006	1.330	−1.515	Amino acids, peptides, and analogues
18	C8H11N3O3S	Resveratrol	N2635	C07065	7.857 ± 0.133	8.019 ± 0.032	8.008 ± 0.058	0.002	1.402	−0.468	Nucleic acids
19	C10H12N4O4	Pantothenic Acid	P2767	C05512	6.612 ± 0.180	7.216 ± 0.146	6.898 ± 0.291	0.007	1.345	−1.576	Nucleic acids
20	C10H12N5O7P	(E)-2-Decylpent-2-Enedioic Acid	P4007	C00942	7.625 ± 0.054	7.450 ± 0.089	6.702 ± 0.547	0.001	1.566	1.148	Nucleic acids
21	C9H12N2O5	Glabrone	P4702	C00526	9.386 ± 0.059	8.771 ± 0.730	7.843 ± 0.168	0.004	1.355	1.665	Nucleic acids
22	C9H13N3O5	Cysteine	P639	C00475	8.301 ± 0.061	7.634 ± 0.048	6.500 ± 0.334	0.000	1.733	2.357	Nucleic acids
23	C11H15N2O8P	Perfluorobutanoic Acid	N2347	C00455	7.706 ± 0.597	6.565 ± 0.525	7.040 ± 0.087	0.001	1.491	3.394	Nucleic acids
24	C14H26N4O11P2	Mycosporine Glutamicol	N3902	C00307	7.734 ± 0.056	7.825 ± 0.077	7.806 ± 0.053	0.030	1.078	−0.274	Nucleic acids
25	C9H12N2O6	Canarione	P3751	C00299	8.212 ± 0.075	5.913 ± 0.461	6.516 ± 0.311	0.000	2.101	5.809	Nucleic acids
26	C10H15N5O10P2	Bromotsitsikammamine B	P5397	C00008	6.447 ± 0.434	7.526 ± 0.684	8.166 ± 0.214	0.019	1.144	−4.629	Nucleic acids
27	C4H8O2	D-Gulonic Acid Gama-Lactone	N1647	C02632	8.339 ± 0.060	9.119 ± 0.432	9.827 ± 0.088	0.003	1.369	−4.329	Organic acids
28	C2H7NO2S	Indazole	P596	C00519	8.552 ± 0.013	8.573 ± 0.040	8.659 ± 0.018	0.015	1.214	−0.220	Organic acids

(*continued on next page*)

Table 3 (*continued*)

No.	Formula	Metabo Name	Alignment ID	KEGGID	EXU2 Log10	EXU4 Log10	EXU6 Log10	*P* value	VIP	Log2 FC	KEGG SuperClass
29	C4H6O5	Gluconasturtiin	P5939	C00497	10.060 ± 0.069	9.348 ± 0.201	9.375 ± 0.185	0.000	2.021	2.198	Organic acids
30	C6H8O5	Cocamidopropylbetaine	P4789	C00322	10.487 ± 0.081	10.410 ± 0.096	8.367 ± 0.513	0.010	1.231	1.217	Organic acids
31	C6H8O7	Methyl Quinoxaline-2-Carboxylate	P2146	C00311	9.133 ± 0.305	9.846 ± 0.132	9.293 ± 0.241	0.039	1.064	−1.455	Organic acids
32	C4H6O4	Prolylyphenylalanine	N3294	C00042	8.459 ± 0.010	8.475 ± 0.045	8.567 ± 0.033	0.031	1.099	−0.219	Organic acids
33	C3H4O3	Lamivudine	N2649	C00022	11.009 ± 0.055	10.614 ± 0.257	10.261 ± 0.167	0.000	1.821	1.612	Organic acids
34	C9H17NO5	Sulfadimethoxine	N3997	C00864	8.086 ± 0.199	8.229 ± 0.267	9.217 ± 0.186	0.045	1.026	−2.892	Vitamins and cofactors
35	C8H11NO3	Trans-Dihydrolisuride	P4753	C00314	9.410 ± 0.129	9.566 ± 0.143	9.661 ± 0.111	0.021	1.216	−0.677	Vitamins and cofactors
36	C8H9NO3	N-Acetyl-L-Phenylalanine	N2248	C00250	9.266 ± 0.126	8.954 ± 0.082	8.791 ± 0.134	0.000	1.770	1.299	Vitamins and cofactors
37	C6H6N2O	L-Beta-Homoproline	P811	C00153	11.048 ± 0.080	10.187 ± 0.757	8.840 ± 0.112	0.000	1.912	2.620	Vitamins and cofactors
38	C10H17N3O6S	Eudesmin	P5474	C00051	8.882 ± 0.056	8.747 ± 0.024	7.873 ± 0.424	0.001	1.538	1.181	Vitamins and cofactors
39	C27H33N9O15P2	Cytidine	N3693	C00016	6.320 ± 0.082	6.437 ± 0.216	7.110 ± 0.089	0.022	1.129	−1.926	Vitamins and cofactors
40	C21H28N7O17P3	Dihydroorotic Acid	N1283	C00006	5.520 ± 0.255	5.905 ± 0.365	6.945 ± 0.221	0.036	1.054	−3.794	Vitamins and cofactors
41	C7H10O5	5-O-Methyllicoricidin	N5127	C00493	8.024 ± 0.131	7.939 ± 0.115	6.221 ± 0.642	0.013	1.228	1.230	Alcohols and polyols
42	C6H14O6	Acetylcholine	P1199	C00794	9.305 ± 0.095	9.378 ± 0.064	9.496 ± 0.053	0.015	1.163	−0.430	Carbohydrates
43	C6H14NO8P	1-Amino-1-Cyclopentanecarboxylic Acid	P810	C00352	8.752 ± 0.075	7.829 ± 0.598	6.494 ± 0.130	0.000	1.912	3.016	Carbohydrates
44	C5H11O8P	Gly-Val	P1840	C00117	9.609 ± 0.061	9.056 ± 0.603	7.210 ± 0.134	0.000	1.589	1.963	Carbohydrates
45	C3H8O3	Sphinganine Related Molecules	P4223	C00116	7.226 ± 0.143	7.115 ± 0.103	7.044 ± 0.094	0.023	1.167	0.520	Carbohydrates
46	C10H12N4O6	Triphenylphosphine Oxide	P3847	C01762	8.102 ± 0.066	7.889 ± 0.207	7.159 ± 0.644	0.009	1.272	1.042	Alkaloids
47	C7H7NO2	Scopolamine Butylbromide	P5940	C01004	8.163 ± 0.080	8.110 ± 0.025	8.061 ± 0.077	0.049	1.031	0.268	Alkaloids
48	C5H4N4O	Panthenol	N2222	C00262	9.589 ± 0.017	9.501 ± 0.039	8.897 ± 0.056	0.002	1.447	0.968	Alkaloids
49	C12H13ClFN3OS	Liriodenine	P4134	C01327	6.844 ± 0.169	7.203 ± 0.309	7.880 ± 0.154	0.019	1.170	−2.739	Homogeneous non-metal compounds
50	H2O3S	Pyridine	P2	C00094	7.786 ± 0.029	7.907 ± 0.038	8.072 ± 0.027	0.000	1.545	−0.703	Homogeneous non-metal compounds
51	H3O4P	Methyl-3-Hydroxybutyric Acid	P598	C00009	10.295 ± 0.029	10.370 ± 0.032	10.487 ± 0.029	0.001	1.490	−0.456	Homogeneous non-metal compounds
52	C25H40N2O6S	N4-Acetylsulfathiazole	P4133	C05951	6.619 ± 0.363	7.402 ± 0.159	7.370 ± 0.117	0.000	1.655	−2.152	Lipids
53	C8H21NO6P	3,5-Diiodo-L-Tyrosine	P5724	C00670	9.778 ± 0.048	9.668 ± 0.195	7.556 ± 0.181	0.010	1.258	1.248	Lipids
54	C20H32O2	Undecanoic Acid	N1813	C00219	9.496 ± 0.164	9.862 ± 0.128	9.684 ± 0.200	0.013	1.233	−0.937	Lipids
55	C9H9NO3	Succinic Acid	P594	C01586	7.396 ± 0.070	6.994 ± 0.376	6.367 ± 0.291	0.001	1.581	1.609	Benzenoids
56	C8H8O	Gallic Acid	P2223	C00601	8.075 ± 0.051	9.958 ± 0.525	10.261 ± 0.349	0.001	1.505	−6.387	Benzenoids
57	C10H13N4O8P	2,3′,4,6-Tetrahydroxybenzophenone	N2989	C00130	10.049 ± 0.015	9.949 ± 0.040	7.999 ± 0.514	0.003	1.419	1.294	Homogeneous metal compounds
58	C7H16NO2	2-Phenylacetamide	P923	C01996	8.041 ± 0.285	8.273 ± 0.056	8.548 ± 0.131	0.026	1.132	−1.057	Hormones and transmitters
59	C13H12N4	L-Arginine	P1846	C16038	8.637 ± 0.084	8.579 ± 0.088	8.510 ± 0.059	0.035	1.047	0.307	Organoheterocyclic
60	C7H5NO4	Methyl Palmitoleate	N3382	C03722	7.964 ± 0.135	8.373 ± 0.262	9.511 ± 0.184	0.038	1.041	−4.291	Organoheterocyclic
61	C26H43NO6	Hypotaurine	P415	C01921	6.912 ± 0.101	7.080 ± 0.106	7.085 ± 0.048	0.002	1.436	−0.553	Steroids
62	C24H40O5	N-Acetyl-O-Methyltyrosine	N2799	C00695	6.651 ± 0.177	6.773 ± 0.368	7.175 ± 0.107	0.019	1.214	−1.259	Steroids
63	C6H6O6	Erucamide	P4718	C05422	8.572 ± 0.112	7.615 ± 0.261	6.893 ± 0.173	0.000	1.997	3.740	Organoheterocyclic compounds
64	C5H14NO	Picropodophyllotoxin	P5746	C00114	10.383 ± 0.047	10.367 ± 0.099	7.361 ± 0.367	0.039	1.056	1.021	Pesticides
65	C9H8O3	Pyrrolnitrin	N3161	C12621	8.881 ± 0.363	9.934 ± 0.094	9.825 ± 0.218	0.000	1.609	−2.834	Phenylpropanoids and polyketides
66	C15H10O7	Cetirizine	P5320	C00389				0.000	1.937	4.284	PK Polyketides

(*continued on next page*)

Table 3 (*continued*)

No.	Formula	Metabo Name	Alignment ID	KEGGID	EXU2 Log10	EXU4 Log10	EXU6 Log10	*P* value	VIP	Log2 FC	KEGG SuperClass
					8.178 ± 0.145	6.105 ± 0.597	6.843 ± 0.573				
67	C6H15NO3	Wogonin	P4278	C06771	7.201 ± 0.260	6.766 ± 0.403	5.656 ± 0.332	0.006	1.330	2.202	Others
68	C14H20O7	N4-Acetylsulfadiazine	N3727	C06046	9.906 ± 0.034	9.956 ± 0.058	10.070 ± 0.051	0.011	1.203	−0.375	Others
69	C9H15N4O8P	Isofraxidin	N2537	C04677	7.887 ± 0.068	7.713 ± 0.040	6.473 ± 0.979	0.002	1.462	1.146	Others
70	C8H9NO	(+)-Dihydrokavain	N2728	C02505	8.901 ± 0.066	8.231 ± 0.132	8.351 ± 0.279	0.000	1.965	1.837	Others
71	C5H11N	Heptadecanoic Acid	N3419	C01746	9.505 ± 0.032	9.375 ± 0.137	9.274 ± 0.144	0.009	1.325	0.519	Others
72	C7H7NO3	Leucylvaline	P2985	C00632	9.191 ± 0.193	9.080 ± 0.099	8.729 ± 0.045	0.011	1.265	0.945	Others
73	C10H12N4O5	Mesotrione	P4736	C00294	10.038 ± 0.038	9.805 ± 0.107	7.797 ± 0.588	0.000	1.700	1.697	Others
74	C2H7NO3S	Histamine Dihydrochloride	P2028	C00245	6.771 ± 0.259	7.450 ± 0.136	7.066 ± 0.108	0.017	1.179	−1.565	Others
75	C20H32N6O12S2	Chasmanine	P5872	C00127	9.295 ± 0.039	9.387 ± 0.068	9.490 ± 0.054	0.002	1.423	−0.493	Others

refrigeration after the beef is divided, with the conversion of glycogen to lactate and the release of ATP (Wicks et al., 2019). The energy metabolic process may change the intra-tissue pH value and promote the hydrolytic degradation of myofibrillar proteins and the structural weakening of highly organized myogenic fibers, affecting muscle shear force (Lomiwes, Farouk, Wu, & Young, 2014). Although pH value and water-holding capacity were not significantly correlated in the present study, previous studies have found that pH value altered myogenic fiber lattice spacing and formed channels within myogenic fibers, promoting water loss (Hughes, Oiseth, Purslow, & Warner, 2014; Xu et al., 2020). Oxidative phosphorylation, a hallmark of protein oxidation processes, is at lower levels in myogenic fibers, contributing to the degradation of myogenic fibers by calpain, alleviating muscle tightness to improve meat shear force and water retention (Li, Li, Du, Shen, & Zhang, 2018). Liu et al. (2022) reported that protein oxidation can alter the hydrophilic and hydrophobic domains of myofibrillar proteins, and the structural domains within and between myofibrils, and also affect protein cross-linking and net protein charge, leading to changes in the structure of muscle fibers and their spatial arrangement and muscle shear force and water-holding capacity. Likewise, muscle oxidation induced the conversion of deoxygenated myoglobin and oxygenated myoglobin to high iron myoglobin, consequently reducing the stability of flesh color (Nam, Hur, Ismail, & Ahn, 2002).

3.6.2. *Amino acid and lipid*

Oxidation of lipids and proteins is the primary factor of sensory, nutritional and edible quality impairment during the refrigeration of beef. As shown in Table 3, the metabolites including amino acids and lipids represented 19.04% of the aggregate. The metabolism of amino acids generated through protein hydrolysis *in vivo* consists of two main aspects, from one perspective, mainly utilized for the synthesis of proteins, peptides, and other nitrogenous substances expected by cells. The other side could be their conversion to α-keto acids through deamination, transamination and decarboxylation either into sugars, lipids, or re-synthesis of certain non-essential amino acids, or oxidized through the tricarboxylic acid cycle (Ma et al., 2021). Alanine, aspartate, glutamate, and threonine experience energy metabolism in the form of pyruvate via the tricarboxylic acid cycle. Conversely, glutamate succinate may be degraded to glycine and acetyl coenzyme A catalyzed by threonine dehydrogenase, which is also involved in the tricarboxylic acid cycle. Furthermore, phenylalanine and tyrosine metabolism furnish synthetic precursors for neurotransmitters and hormones. Glycine, serine and threonine metabolism are auxiliary procedures within energy metabolism, and glycine is associated with the biosynthesis of glutathione and creatine, which play imporatnt roles in antioxidant defense and energy production, respectively (Zhang et al., 2022). Serine is an intermediate in several metabolic pathways, such as purine synthesis and methionine cycle, depending on the glycolytic intermediate 3-phosphoglycerate or glycine metabolism, and its metabolism promotes lipid metabolism. Boerboom, van Kempen, Navarro-Villa, and Pérez-Bonilla (2018) suggested that hypoxia may be a significant factor in the induction of lipid metabolism and fatty acid accumulation, which can lessen or dispose of mitochondrial β-oxidation, tricarboxylic acid cycle and respiratory chain activity, thus enhancing lipid metabolic processes and prompting the gathering of fatty acids and their derivatives. The metabolism of glutathione and the metabolism of taurine and hypotaurine predominantly increase antioxidant defense.

3.6.3. *Ferroptosis and gap junction*

The connection between apoptosis and meat quality is well defined, while the process of cellular ferroptosis in the metabolic pathway is distinct. Ferroptosis, a new form of cell death, varies from another cell death-like autophagy or senescence, and is fundamentally characterized by iron homeostasis, iron homeostasis and iron-dependent lipid peroxidation. Consequently, at least 40% of the muscle fiber type in beef muscle fibers, viewed as red strands, is β-red, with significant amounts of iron ions (Liu et al., 2022). The accumulation of iron and reactive oxygen species as a central part of iron death reduces cysteine uptake, depletes glutathione and releases arachidonic acid, thus inhibiting the activity of the cysteine or glutamate reverse transport system and glutathione peroxidase 4 (Liu et al., 2022). The decrease in the content of glutathione, a metabolite involved in the iron death process, increased the concentration of L-glutamate, glutathione (oxidized form), and arachidonic acid, suggesting an enhancement of ferroptosis process. Gap junctions (GJ) are intercellular membrane channels that mediate direct communication through the trading of cytoplasmic signaling molecules between neighboring cells. Loss of function as a GJ may lead to apoptosis and necrosis (Li, Shi, et al., 2021). GJ intercellular communication is associated with decisions about cell death under oxidative conditions. The target cells produce death factors, which are secreted into the extracellular space or propagate through GJ towards neighboring cells to promote apoptosis through intercellular pro-apoptotic signaling (Luo et al., 2015). The ferroptosis found in this study during beef refrigeration was complementary to the new form of apoptosis, and GJ was similarly seldom reported in meat studies. The complex and diverse processes of iron death and GJ need further investigations.

Table 4
Screening for significant metabolic pathways associated with meat quality (42).

No.	ID	Description	*q* value	KEGG ID	Second Class	Top Class	UP	DOWN
1	bta04714	Thermogenesis	0.043	C00008/C00942/C00116	Environmental adaptation	Organismal Systems	2	1
2	bta04664	Fc epsilon RI signaling pathway	0.009	C00219/C00388/C05951	Immune system	Organismal Systems	0	3
3	bta04611	Platelet activation	0.016	C00219/C00008/C00942	Immune system	Organismal Systems	1	2
4	bta04918	Thyroid hormone synthesis	0.001	C00127/C00117/C00051/C01060/C00006	Endocrine system	Organismal Systems	3	2
5	bta04923	Regulation of lipolysis in adipocytes	0.016	C00219/C00942/C00116	Endocrine system	Organismal Systems	2	1
6	bta04925	Aldosterone synthesis and secretion	0.040	C00219/C00942/C00006	Endocrine system	Organismal Systems	1	2
7	bta04922	Glucagon signaling pathway	0.055	C00022/C00311/C00042	Endocrine system	Organismal Systems	1	2
8	bta04911	Insulin secretion	0.070	C00022/C01996	Endocrine system	Organismal Systems	1	1
9	bta04921	Oxytocin signaling pathway	0.070	C00219/C00942	Endocrine system	Organismal Systems	1	1
10	bta04974	Protein digestion and absorption	0.000	C00025/C00148/C00483/C00062/C02632/C01746/C00082/C00388/C01327/C00064	Digestive system	Organismal Systems	3	7
11	bta04976	Bile secretion	0.023	C00114/C00051/C01996/C07065/C00942/C01921/C00695	Digestive system	Organismal Systems	3	4
12	bta04977	Vitamin digestion and absorption	0.035	C00153/C00250/C00864/C00016	Digestive system	Organismal Systems	2	2
13	bta04978	Mineral absorption	0.068	C00009/C00148/C00064	Digestive system	Organismal Systems	0	3
14	bta00970	Aminoacyl-tRNA biosynthesis	0.023	C00025/C00148/C00062/C00082/C00064	Translation	Genetic Information Processing	2	3
15	bta00360	Phenylalanine metabolism	0.000	C00022/C00601/C12621/C00082/C02505/C00042/C03519/C05332/C01586	Amino acid metabolism	Metabolism	4	5
16	bta00250	Alanine, aspartate and glutamate metabolism	0.001	C00022/C00025/C00042/C00352/C03406/C00064	Amino acid metabolism	Metabolism	3	3
17	bta00260	Glycine, serine and threonine metabolism	0.006	C00719/C00022/C00114/C00258/C01026/C06231	Amino acid metabolism	Metabolism	4	2
18	bta00220	Arginine biosynthesis	0.009	C00025/C00062/C03406/C00064	Amino acid metabolism	Metabolism	2	2
19	bta00350	Tyrosine metabolism	0.029	C00022/C06046/C00483/C00082/C00042/C01060	Amino acid metabolism	Metabolism	3	3
20	bta00760	Nicotinate and nicotinamide metabolism	0.002	C00022/C00153/C03722/C00042/C01004/C00455/C00006	Metabolism of cofactors and vitamins	Metabolism	4	3
21	bta00750	Vitamin B6 metabolism	0.017	C00314/C00117/C00250/C00064	Metabolism of cofactors and vitamins	Metabolism	2	2
22	bta00230	Purine metabolism	0.001	C00130/C00294/C00262/C00117/C01762/C00008/C04677/C00942/C00064/C05512	Nucleotide metabolism	Metabolism	7	3
23	bta00190	Oxidative phosphorylation	0.021	C00009/C00042/C00008	Energy metabolism	Metabolism	0	3
24	bta00920	Sulfur metabolism	0.086	C00042/C00094/C00245	Energy metabolism	Metabolism	0	3
25	bta00480	Glutathione metabolism	0.000	C00025/C01879/C00127/C00051/C05422/C00669/C00006	Metabolism of other amino acids	Metabolism	3	4
26	bta00430	Taurine and hypotaurine metabolism	0.002	C00022/C00025/C00519/C00094/C00245	Metabolism of other amino acids	Metabolism	1	4
27	bta00471	D-Glutamine and D-glutamate metabolism	0.078	C00025/C00064	Metabolism of other amino acids	Metabolism	0	2
28	bta01240	Biosynthesis of cofactors	0.000	C00022/C00153/C00322/C00025/C00483/C00130/C00311/C00314/C00127/C00082/C00117/C03722/C00250/C00632/C00864/C00051/C00008/C00493/C00064/C00016/C00669/C00006	Global and overview maps	Metabolism	10	12
29	bta01230	Biosynthesis of amino acids	0.002	C00022/C00322/C00025/C00148/C00062/C00311/C00082/C00117/C00493/C03406/C00064	Global and overview maps	Metabolism	7	4
30	bta00630	Glyoxylate and dicarboxylate metabolism	0.013	C00022/C00025/C00258/C00311/C00042/C00064	Carbohydrate metabolism	Metabolism	2	4
31	bta00020	Citrate cycle (TCA cycle)	0.032	C00022/C00311/C00042	Carbohydrate metabolism	Metabolism	1	2
32	bta00650	Butanoate metabolism	0.055	C00022/C00025/C00497/C00042	Carbohydrate metabolism	Metabolism	2	2
33	bta00564	Glycerophospholipid metabolism	0.029	C00114/C00670/C01996/C00307/C06771	Lipid metabolism	Metabolism	3	2
34	bta04540	Gap junction	0.063	C00025/C00942	Cellular community - eukaryotes	Cellular Processes	1	1
35	bta04216	Ferroptosis	0.004	C00025/C00219/C00127/C00051/C00669	Cell growth and death	Cellular Processes	1	4
36	bta05230	Central carbon metabolism in cancer	0.000	C00022/C00025/C00148/C00062/C00311/C00082/C00042/C00064	Cancer: overview	Human Diseases	3	5
37	bta05208	Chemical carcinogenesis - reactive oxygen species	0.086	C00127/C00051/C16038/C00006	Cancer: overview	Human Diseases	2	2
38	bta05415	Diabetic cardiomyopathy	0.002			Human Diseases	3	3

(*continued on next page*)

Table 4 (*continued*)

No.	ID	Description	*q* value	KEGG ID	Second Class	Top Class	UP	DOWN
				C00022/C00794/C00127/C00051/C00352/C00006	Cardiovascular disease			
39	bta02010	ABC transporters	0.000	C00719/C00009/C00114/C00025/C00148/C00062/C00294/C00794/C00526/C00051/C00475/C01762/C00299/C00064/C00245/C00116/C05512	Membrane transport	Environmental Information Processing	9	8
40	bta04080	Neuroactive ligand-receptor interaction	0.002	C00025/C00483/C00388/C01996/C00008/C05951/C00245	Signaling molecules and interaction	Environmental Information Processing	0	7
41	bta04152	AMPK signaling pathway	0.009	C00022/C00008/C00389/C04677	Signal transduction	Environmental Information Processing	3	1
42	bta04068	FoxO signaling pathway	0.021	C00025/C00008	Signal transduction	Environmental Information Processing	0	2

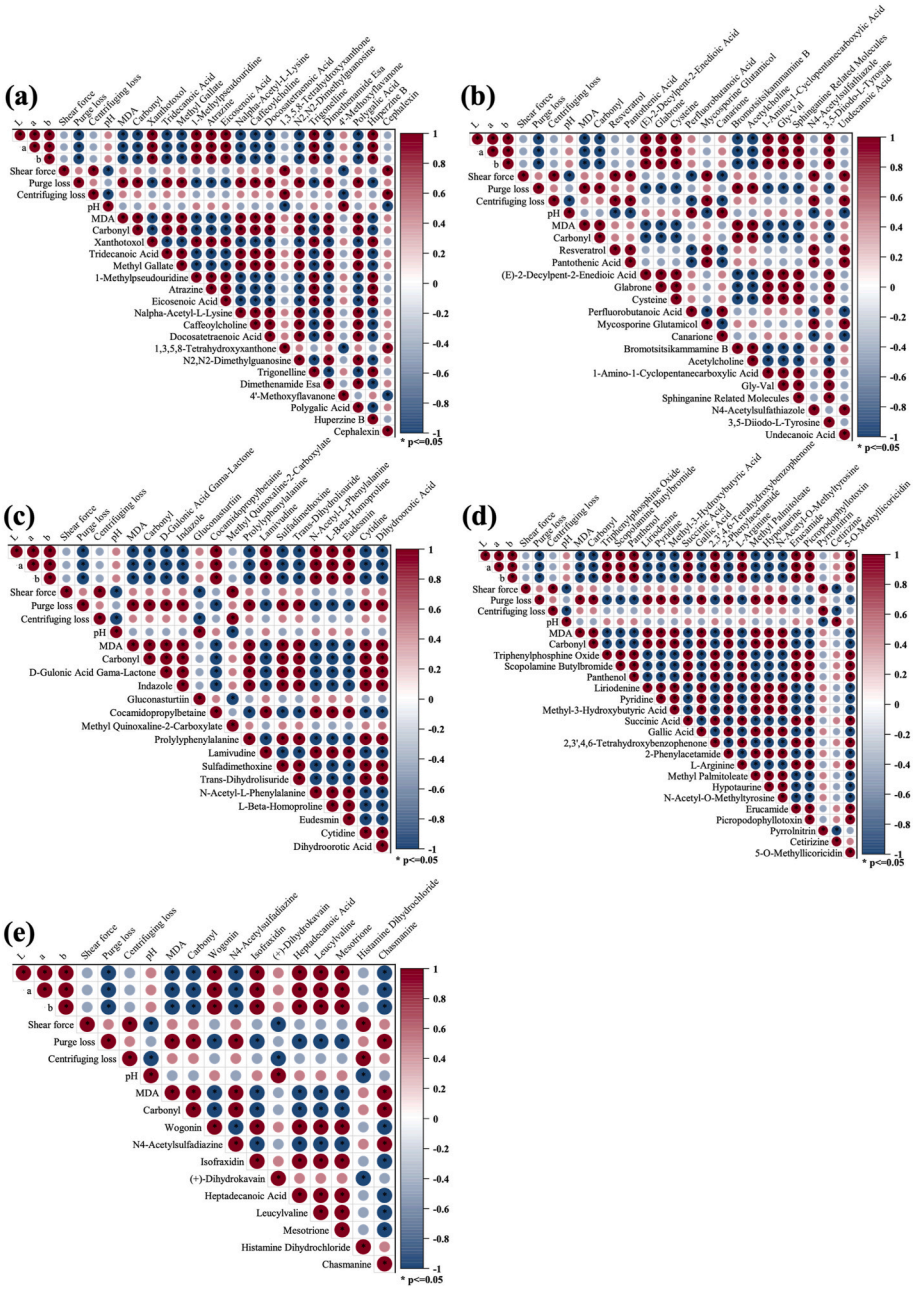

Fig. 5. Correlation analysis of meat quality with DMs. (a) Correlation analysis of meat quality with amino acids, peptides, and analogues. (b) Correlation analysis of meat quality with nucleic acids, lipids and carbohydrates. (c) Correlation analysis of meat quality with organic acids, vitamins and cofactors. (d) Correlation analysis of meat quality with alcohols and polyols, alkaloids, Homogeneous non-metal compounds, benzenoids, hormones and transmitters, organoheterocyclic, Steroids, organoheterocyclic compounds, pesticides, phenylpropanoids and polyketides and PK polyketides. (e) Correlation analysis of meat quality with other DMs.

3.6.4. Other metabolites and metabolic pathways

Nucleosides and nucleotides have many physiological functions, including direct involvement in the metabolism of other substances through different biochemical processes. Nonetheless, only L-glutamine and ADP levels increased during nucleotide metabolism, and ATP-related precursors, including myosin 5′-monophosphate, hypoxanthine and xanthine, showed downregulation, suggesting that nucleotide metabolic processes were also related to energy metabolism (Wen, Liu, & Yu, 2020). Both hypoxanthine and xanthine were products of purine metabolism and may be markers of oxidative stress, and both produce reactive oxygen species as they are utilized as substrates for cofactors in the form of O_2 to produce superoxide (O_2^-). Additionally, purine metabolism is mainly involved in adenine nucleotide metabolism sustaining ATP levels in energy metabolism (Beauclercq et al., 2016). Enhancements in purine metabolic processes, accumulation of ADP during metabolism, and decreases in hypoxanthine and xanthine levels detected by differential metabolites also suggested that purine metabolism was an equally significant complementary pathway for energy metabolism. The biosynthesis of amino acid tRNA, adenosine triphosphate-binding transporter protein and amino acid tRNA were all processes of basal cellular metabolism. The AMPK signaling pathway was an overwhelmingly essential metabolic pathway regulating energy homeostasis, and the FoxO signaling pathway was considered a crucial metabolic process that inhibits cell proliferation and induces apoptosis. These metabolic pathways directly or indirectly affect muscle tissues or cellular states, affecting the fundamental properties of muscle.

4. Conclusions

In the present study, 877 metabolites and 433 DMs were identified in three groups of EXU samples by a metabolomics approach, indicating the promising application of EXU as an experimental sample for meat quality and biochemical analysis. A total of 75 DMs associated with muscle quality were identified in EXU samples, and KEGG metabolic analysis indicated that synergistic effects of various metabolic pathways and enhanced oxidative state processes resulted in the induction of altered muscle cell states. The results affirmed the potential of EXU samples for application in meat quality analysis while clarifying the adverse effects of muscle oxidation and apoptosis on meat quality. This study may be helpful for the development of more precise and effective meat quality control strategies in the future. Meat quality is influenced by many factors, such as storage conditions and microbial activity, our study only gave an insight into changes within the muscle through exudate, so a more comprehensive study is needed.

Funding

This study was financially supported by the Ningxia Natural Science Foundation (2021AAC03013, 2022AAC02021).

CRediT authorship contribution statement

Jun Liu: Conceptualization, Data curation, Formal analysis, Investigation, Methodology, Resources, Validation, Visualization, Writing – original draft, Writing – review & editing. **Ziying Hu:** Data curation, Formal analysis, Investigation, Writing – original draft, Writing – review & editing. **Anran Zheng:** Investigation. **Qin Ma:** Writing – review & editing. **Dunhua Liu:** Conceptualization, Formal analysis, Funding acquisition, Investigation, Project administration, Supervision, Visualization.

Declaration of competing interest

The authors declare no conflict of interest.

Data availability

No data was used for the research described in the article.

Acknowledgments

We thank the Ningxia Provincial Natural Science Foundation (2021AAC03013, 2022AAC02021) for providing financial support for this project. The authors would like to thank Shanghai Bioprofile Co., Ltd. for providing technical support for UPLC-ESI-Q-Orbitrap-MS metabolomics.

References

An, R., Nickols-Richardson, S., Alston, R., Shen, S., & Clarke, C. (2019). Total, fresh, lean, and fresh lean beef consumption in relation to nutrient intakes and diet quality among US adults, 2005-2016. *Nutrients, 11*(3).

Ayaka, N., Yuri, M., Hajime, T., Kota, O., Takashi, K., & Bon, K. (2022). Dynamics of microbiota in the imported beef primal cuts during storage at different chilled temperatures. *Bioscience, Biotechnology, and Biochemistry, 86*(8), 1106–1113.

Beauclercq, S., Nadal-Desbarats, L., Hennequet-Antier, C., Collin, A., Tesseraud, S., Bourin, M., et al. (2016). Serum and muscle metabolomics for the prediction of ultimate pH, a key factor for chicken-meat quality. *Journal of Proteome Research, 15*(4), 1168–1178.

Benjamin, W. B. H., Cassius, E. O. C., Stephen, M., Matthew, J. K., & David, L. H. (2017). Effect of long term chilled (up to 5 weeks) then frozen (up to 12 months) storage at two different sub-zero holding temperatures on beef: 1. Meat quality and microbial loads. *Meat Science, 133*, 133–142.

Boerboom, G., van Kempen, T., Navarro-Villa, A., & Pérez-Bonilla, A. (2018). Unraveling the cause of white striping in broilers using metabolomics. *Poultry Science, 97*(11), 3977–3986.

Bowker, B., Gamble, G., & Zhuang, H. (2016). Exudate protein composition and meat tenderness of Broiler breast fillets. *Poultry Science, 95*(1), 133–137.

Castejón, D., García-Segura, J. M., Escudero, R., Herrera, A., & Cambero, M. I. (2015). Metabolomics of meat exudate: Its potential to evaluate beef meat conservation and aging. *Analytica Chimica Acta, 901*, 1–11.

Coll Cárdenas, F., Andrés, S., Giannuzzi, L., & Zaritzky, N. (2011). Antimicrobial action and effects on beef quality attributes of a gaseous ozone treatment at refrigeration temperatures. *Food Control, 22*(8), 1442–1447.

Di Luca, A., Elia, G., Mullen, A. M., & Hamill, R. M. (2013). Monitoring post mortem changes in porcine muscle through 2-D DIGE proteome analysis of Longissimus muscle exudate. *Proteome Science, 11*(1), 9.

Dransfield, E. (1994). Optimisation of tenderisation, ageing and tenderness. *Meat Science, 36*, 105–121.

Fang, J. Y., Feng, L. F., Lu, H. X., & Zhu, J. L. (2022). Metabolomics reveals spoilage characteristics and interaction of Pseudomonas lundensis and Brochothrix thermosphacta in refrigerated beef. *Food Research International, 156*, Article 111139.

Hughes, J. M., Oiseth, S. K., Purslow, P. P., & Warner, R. D. (2014). A structural approach to understanding the interactions between colour, water-holding capacity and tenderness. *Meat Science, 98*(3), 520–532.

Kim, G., Jeong, T., Yang, H., Joo, S., Hur, S. J., & Jeong, J. (2015). Proteomic analysis of meat exudates to discriminate fresh and freeze-thawed porcine longissimus thoracis muscle. *LWT - Food Science and Technology, 62*(2), 1235–1238.

Kim, G., Jung, E., Lim, H., Yang, H., Joo, S., & Jeong, J. (2013). Influence of meat exudates on the quality characteristics of fresh and freeze-thawed pork. *Meat Science, 95*(2), 323–329.

Li, Z., Li, M., Du, M., Shen, Q. W., & Zhang, D. (2018). Dephosphorylation enhances postmortem degradation of myofibrillar proteins. *Food Chemistry, 245*, 233–239.

Li, C., Shi, L., Peng, C., Yu, G., Zhang, Y., & Du, Z. (2021). Lead-induced cardiomyocytes apoptosis by inhibiting gap junction intercellular communication via autophagy activation. *Chemico-Biological Interactions, 337*, Article 109331.

Liu, J., Hu, Z., Liu, D., Zheng, A., & Ma, Q. (2023). Glutathione metabolism-mediated ferroptosis reduces water-holding capacity in beef during cold storage. Food Chemistry, 398, 133903.

Liu, J., Liu, D., Wu, X., Pan, C., Wang, S., & Ma, L. (2022). TMT quantitative proteomics analysis reveals the effects of transport stress on iron metabolism in the liver of chicken. *Animals, 12*(1), 52.

Liu, J., Liu, D., Zheng, A., & Ma, Q. (2022). Haem-mediated protein oxidation affects water-holding capacity of beef during refrigerated storage. *Food Chemistry, X*, Article 100304.

Li, D., Zhang, H., Ma, L., Tao, Y., Liu, J., & Liu, D. (2021). Effects of ficin, high pressure and their combination on quality attributes of post-rigor tan mutton. *LWT - Food Science and Technology, 137*, Article 110407.

Lomiwes, D., Farouk, M. M., Wu, G., & Young, O. A. (2014). The development of meat tenderness is likely to be compartmentalised by ultimate pH. *Meat Science, 96*(1), 646–651.

Luo, C., Yuan, D., Yao, W., Cai, J., Zhou, S., Zhang, Y., et al. (2015). Dexmedetomidine protects against apoptosis induced by hypoxia/reoxygenation through the inhibition of gap junctions in NRK-52E cells. *Life Sciences, 122*, 72–77.

Mariana, U., David, M., & Mario, E. (2014). Temperature of frozen storage affects the nature and consequences of protein oxidation in beef patties. *Meat Science, 96*(3), 1250–1257.

Ma, B., Zhang, L., Li, J., Xing, T., Jiang, Y., & Gao, F. (2021). Heat stress alters muscle protein and amino acid metabolism and accelerates liver gluconeogenesis for energy supply in broilers. *Poultry Science, 100*(1), 215–223.
Nam, K. C., Hur, S. J., Ismail, H., & Ahn, D. U. (2002). Lipid oxidation, volatiles, and color changes in irradiated raw Turkey breast during frozen storage. *Journal of Food Science, 67*(6), 2061–2066.
Nour, V. (2022). Effect of sour cherry or plum juice marinades on quality characteristics and oxidative stability of pork loin. *Foods, 11*(8), 1088.
Pereira, T. L., Fernandes, A., Oliveira, E. R., Cnsolo, N., & Gandra, J. R. (2020). Serum metabolomic fingerprints of lambs fed chitosan and its association with performance and meat quality traits. *Animal, 14*(9), 1–12.
Wang, C., Li, X., Zhao, X., Bi, H., & Xie, J. (2022). The investigation of storage situation of fish muscle via the analysis of its exudate by MALDI-TOF MS. *Food Chemistry, 373*, Article 131450.
Wen, D., Liu, Y., & Yu, Q. (2020). Metabolomic approach to measuring quality of chilled chicken meat during storage. *Poultry Science, 99*(5), 2543–2554.
Wicks, J., Beline, M., Gomez, J. F., Luzardo, S., Silva, S. L., & Gerrard, D. (2019). Muscle energy metabolism, growth, and meat quality in beef cattle. *Agriculture, 9*(9), 195.
Xing, T., Zhao, X., Xu, X., Li, J., Zhang, L., & Gao, F. (2020). Physiochemical properties, protein and metabolite profiles of muscle exudate of chicken meat affected by wooden breast myopathy. *Food Chemistry, 316*, Article 126271.
Xu, D., Wang, Y., Jiao, N., Qiu, K., Zhang, X., Wang, L., et al. (2020). The coordination of dietary valine and isoleucine on water holding capacity, pH value and protein solubility of fresh meat in finishing pigs. *Meat Science, 163*, Article 108074.
You, Y., Her, J., Shafel, T., Kang, T., & Jun, S. (2020). Supercooling preservation on quality of beef steak. *Journal of Food Engineering, 274*, Article 109840.
Yu, Q., Cooper, B., Sobreira, T., & Kim, Y. H. B. (2021). Utilizing pork exudate metabolomics to reveal the impact of aging on meat quality. *Foods, 10*(3), 668.
Yu, Q., Wu, W., Tian, X., Jia, F., Xu, L., Dai, R., et al. (2017). Comparative proteomics to reveal muscle-specific beef color stability of Holstein cattle during post-mortem storage. *Food Chemistry, 229*, 769–778.
Zhang, X., Han, L., Hou, S., Raza, S., Wang, Z., Yang, B., et al. (2022). Effects of different feeding regimes on muscle metabolism and its association with meat quality of Tibetan sheep. *Food Chemistry, 374*, Article 131611.
Zhou, C., Wang, C., Dai, C., Bai, Y., Yu, X., Li, C., et al. (2019). iTRAQ-based quantitative proteomic characterizes the salting exudates of Jinhua ham during the salting process. *Food Control, 100*, 189–197.